Switched Reluctance Motor for Electric Submersible Pump

Robert Adams[1,*], Jinjiang Xiao[2], Michael Cross[1], Max Deffenbaugh[1]
[1]Aramco Americas: Aramco Research Center – Houston, Aramco Services Company, USA,
Email: robert.adams@aramcoamericas.com
[*] Corresponding author
[2]Expl. and Petroleum Engineering Advanced Research Center (EXPEC ARC), Saudi Aramco, Saudi Arabia
Email: jinjiang.xiao@aramco.com

Abstract: **Switched reluctance motors may be advantageous when used as the primary motor for an electric submersible pump system. They are less susceptible to jamming failures due to their high starting torque and ability to reverse direction. Driving these motors requires well-timed pulse waveforms and precise control of the motor based on its rotational position. In general, voltage-based sensing and control systems at the surface see highly unpredictable waveforms with excessive ringing behaviour due to the impedance characteristics of the long cabling between the surface controller and the downhole motor system. In this work, a system is detailed which monitors the current waveforms on the motor coil excitation conductors at the surface as a source of motor performance feedback and control. State-space modelling of the system shows stable current waveforms at the surface controller for both short and long interconnect cable systems. A laboratory demonstration of the surface controller, interconnect cabling, and motor system is shows excellent agreement with the current and voltage waveforms predicted by the state-space system model.**

Keywords: **Switched Reluctance Motor, Electric Submersible Pump, Motor Control, Cable Simulation.**

I. INTRODUCTION

Oil production is often accelerated by deploying an electric submersible pump (ESP) deep in the well. These pumps are usually powered by an electric motor at the bottom of cables which can be in excess of one mile long. Traditional ESP systems for oil production use three-phase induction motors (IM). A recent industrial trend is to use a permanent magnet motor (PMM) in place of the induction motor for reduced motor size and increased motor efficiency and reliability, but added cost due to the use of rare earth permanent magnets. ESP failures are very expensive to repair, and one failure mode is jamming [1-3], where the motor is not able to rotate the pump. IM and PMM based systems are not easily cleared of a jamming failure, where reverse rotation and/or large starting torques are required.

A potential alternative to IMs and PMMs is a switched reluctance motor (SRM), which is capable of high-speed, high power density and efficiency. SRMs offer higher starting torques than induction motors [4-7], making them less susceptible to jamming, so it would be desirable to replace induction motors with switched reluctance motors in ESP applications. Additionally, they do not require rare earth materials like PMMs. There are challenges with using SRMs, in that these systems are powered by pulse waveforms with energy content much higher than the rotation rate, which may be difficult to provide over long cables [8,9]. The timing of the pulse waveforms must be carefully synchronized to rotor position, which may be difficult to achieve without high-bandwidth data from downhole sensors [10-13]. One approach to solve the control challenge is to incorporate downhole high frequency power electronics and combine multiple modular designs. Considering industry experiences, however, this approach will reduce the reliability of these systems. A more reliable solution is to move all high-speed measurement and control electronics to the surface, and control one single high horsepower motor downhole. This presents a unique challenge for downhole artificial lift applications due to the long cable length required between the surface equipment and the downhole motor system. This paper describes a solution to the monitoring and control problem with a surface system driving a downhole SRM over long lengths of cable.

II. SWITCHED RELUCTANCE MOTOR SURFACE CONTROL

Electric motor systems for powering submersible pumps use PMMs or IMs. In a PMM motor, torque is produced when permanent magnets on the rotor are attracted to magnetic fields produced by currents in the stator coils. Motor controllers for permanent magnet motors generally use variable frequency drives where three sinusoidal drive signals are produced 120 degrees out of phase by pulse width modulation. Motor speed is controlled by the frequency of the driving waveforms, and the driving waveforms must be

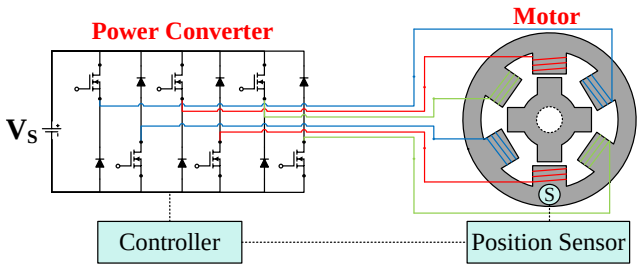

Fig. 1. Standard SRM System with integrated position sensor at the motor. The power converter (left) is modulated by the controller (bottom), and successively transmits energy from power source Vs. A switched reluctance motor with integrated position sensor (right) is driven by the controller and power converter. A position sensor 'S' integrated into the downhole motor system provides feedback to the controller.

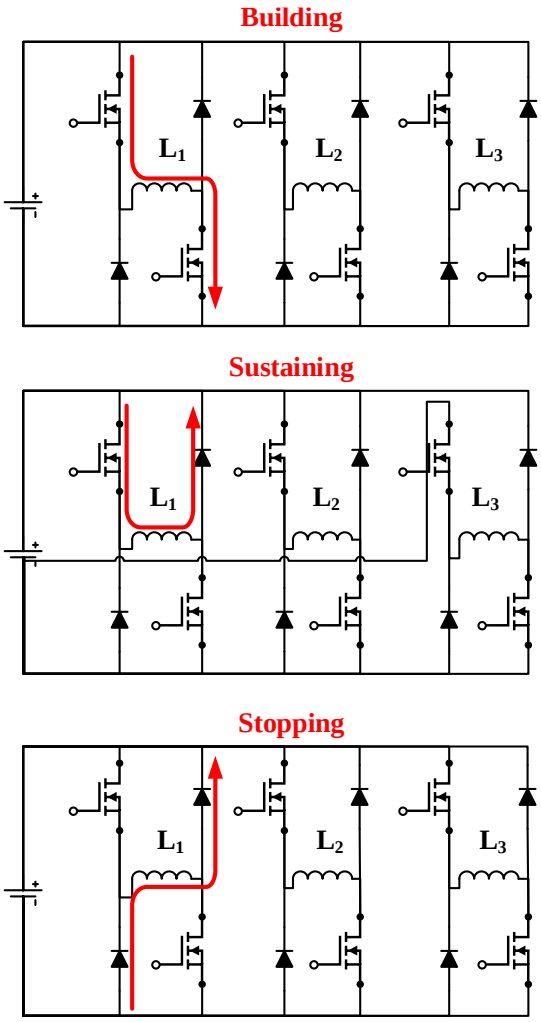

Fig. 2. Asymmetric half bridge power converter topology. Three states of operation for motor coil L1 are shown: current building (top), current sustaining (middle), and current stopping (bottom).

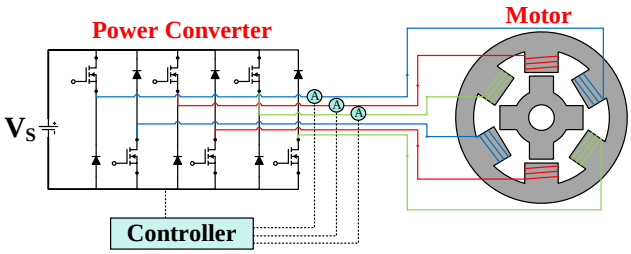

Fig. 3. Proposed SRM controller system with current sensing on inductor coil lines. There are no position sensing electronics are integrated into the motor assembly. Current sensors 'A', positioned at the surface power converter electronics, provide feedback to the controller.

synchronous with the rotor position so that the fields from the stator coils are produced at the right times and the right polarities to advance the rotor. There are limitations on how fast PMM motors can be driven. The spinning permanent magnets on the rotor induce a back-EMF in the stator coils. The drive voltage applied must exceed the back-EMF sufficiently to drive current through the stator coils. Since the back-EMF increases with rotation rate, the maximum voltage limitations of the driver impose a maximum speed limitation on the motor. It is desirable to operate ESPs at high rotation rates as this enables a pumping unit of a given size to apply more energy to lifting the wellbore fluids. Thus the speed limitation of PMM motors is a disadvantage for ESP applications.

Most motor systems for powering submersible pumps are based on alternating current (AC) induction motors. In an AC induction motor, an alternating current in the stator coils generates an alternating magnetic field which induces eddy currents in the rotor, which is typically made of steel but not permanently magnetized. The eddy currents produce their own magnetic field from the rotor which is attracted to the magnetic field from the stator creating a torque which turns the rotor. Induction motors are driven asynchronously, in that the rotation rate of the rotor is slower than the rotation rate of the field from the stator coils. The torque produced by the induction motor depends on the amplitude of the current applied to the stator coils and the slip factor or percent difference between the rotation rates of the stator field and the rotor. In most modern motor systems, a variable frequency drive is used to produce three sinusoidal drive signals of an optimized frequency and amplitude to provide the torque required to sustain rotation at the desired rate. The torque of induction motors is relatively low when the rotor is stalled. This is a disadvantage for ESP applications, in that there is limited torque for breaking free if the pump becomes jammed by sediments or heavy hydrocarbons [14].

In an SRM, torque is generated by varying the magnetic flux linkage between the permeable rotor and the stator by progressively energizing the poles of the stator to repeatedly align the poles of the rotor and stator. In this case, the rotor is made entirely of a permeable material, and does not contain windings or permanent magnets [15]. Motor controllers for this motor type use current-switching circuits to drive the motor similar to permanent magnet motor controllers. Motor speed is synchronously controlled by the frequency of the driving waveforms [16]. Since SRMs have no permanent magnets, they are free of the back-EMF speed limitation of PMAC motors, making them capable of very high speed operation. They are also able to apply full torque when the rotor is stalled, enabling them to break free from jams that could stop induction motors.

In a typical SRM system, Fig. 1, power converter electronics issue well-timed voltage pulse waveforms to coils in the motor stator in such a way as to successively move the rotor. Each coil is sequentially operated in three states: current building, current sustaining, and current stopping. Fig. 2 shows the three states of the coils in an asymmetric half-bridge power converter topology. During the current building state, voltage is applied to the coil and current develops. The rotor moves toward the energized coil. During the current sustaining state, the stored energy in the magnetic field of the coil maintains current within the coil until resistances in the wire dissipate the energy. The rotor continues to move near the coil through its own rotational inertia. During the current stopping state, an instantaneous counter-emf voltage spike that drains current out through the diodes, rapidly decreasing the current to zero. There is no longer an attractive force between this coil and the rotor. At

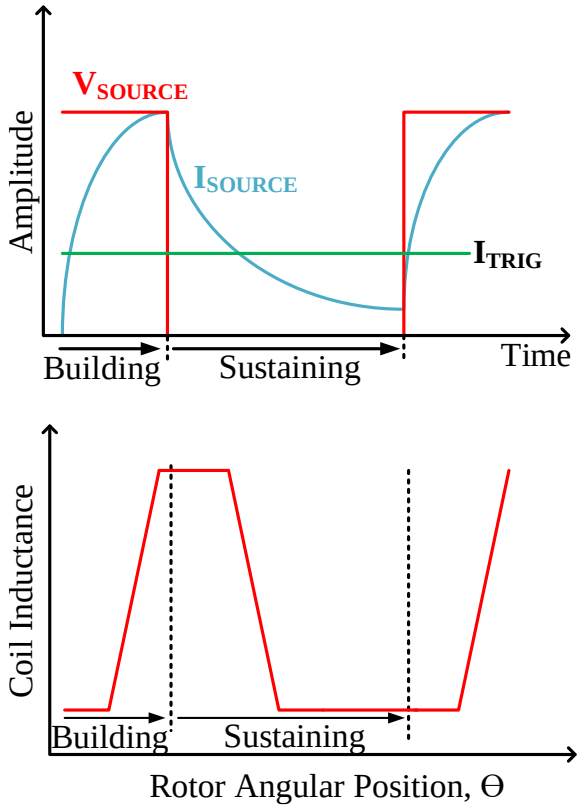

Fig. 4. (Top) Voltages issued by the power source and the resulting current draw of the source during the building and sustaining coil states in the proposed control scheme. I_{TRIG} is a current threshold level for changing coil states. (Bottom) Inductance of a motor coil as a function of rotor angular position during the building and sustaining coil states.

this point in the sequence, the next coil is excited and the pulse sequence repeats.

The timing of these pulse waveforms is controlled by monitoring the position of the rotor throughout the pulsing sequence. This method of monitoring the rotor position enables closed loop motor control of rotational speed and direction. This requires including electronics to monitor the position of the motor downhole. This implies the use of complex electronic devices in the harsh environment the ESP is deployed into with added reliability risks, as well as communication methods to bring information from the rotor position measurements to the motor control system – potentially adding more conductor cables between the surface and downhole, and the added reliability risks that come with this.

Control of an SRM system can be vastly simplified by monitoring the pulse waveform current into each coil rather than directly monitoring rotor position, Fig. 3. It is important to note that the relationship in voltage between the power converter and the voltage induced in the motor coil is highly nonlinear, and susceptible to large swings due to impedances throughout the motor/cable/coil system and the frequency content of the voltage pulse waveform. But, the current sourced by the power converter is nearly identical to the current into the motor coil. There is a direct relationship between the current supplied by the power converter electronics, the effect of the cable impedances, and the motor coil position.

In this proposed method, the current supplied by the surface power converter is monitored continuously, and the change of state in the pulsing sequence is based on threshold crossings in measured current during the building, sustaining, and stopping state for each coil. Fig. 4 top shows the relationship between power converter current, pulse sequence state, and current control thresholds. Fig. 4 bottom shows the relationship between the rotor position and the coil inductance. As the rotor moves, the coil inductance will vary due to the angular position of the rotor due to changes in mutual inductance between the rotor and the coil. If the rotor and coil are unaligned then the coil inductance is at a minimum, and if the rotor and state are exactly aligned then the coil inductance is at a maximum. The current through the coil is:

$$I_{SOURCE}(\theta) \approx I_{COIL}(\theta) = \int \frac{v_{COIL}(\theta)}{L_{COIL}(\theta)} d\theta \qquad (1)$$

where $I_{SOURCE\ (\theta)}$ is the current supplied by the power converter as a function of angular position, $I_{COIL}(\theta)$ is the current through the motor coil as a function of angular position, $v_{COIL}(\theta)$ is the voltage across the coil as a function of angular position, $L_{COIL}(\theta)$ is the inductance of the motor coil as a function of angular position, and θ is the angular position of the rotor with respect to the coil being energized.

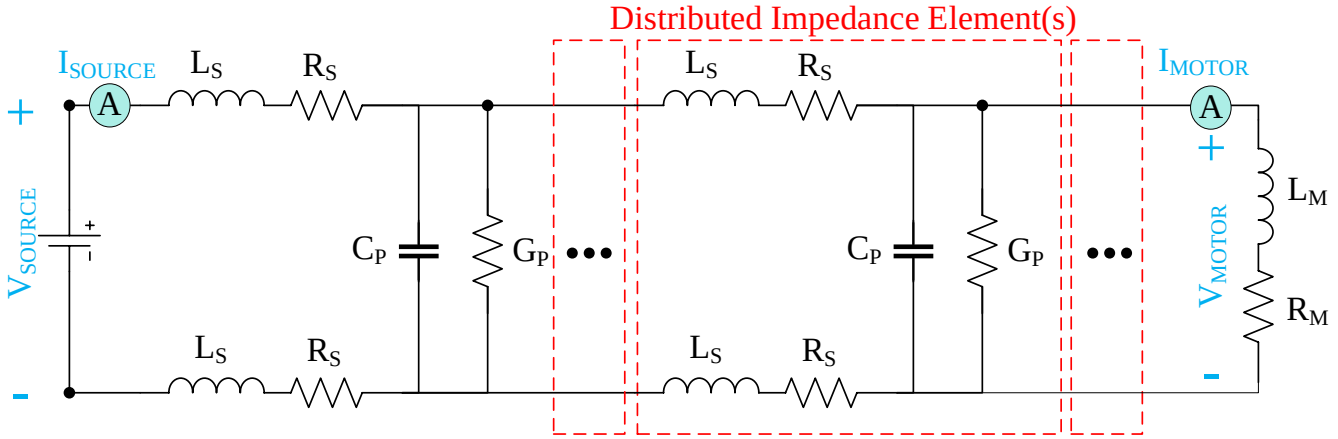

Fig. 5. Distributed cable impedance model for the finite difference simulation of cable voltages and currents. V_{SOURCE}, I_{SOURCE}, V_{MOTOR}, and I_{MOTOR} measurement locations are indicated in blue. The distributed impedance element is repeated continuously to model the distributed impedance behavior of the interconnect cable between the source and the motor.

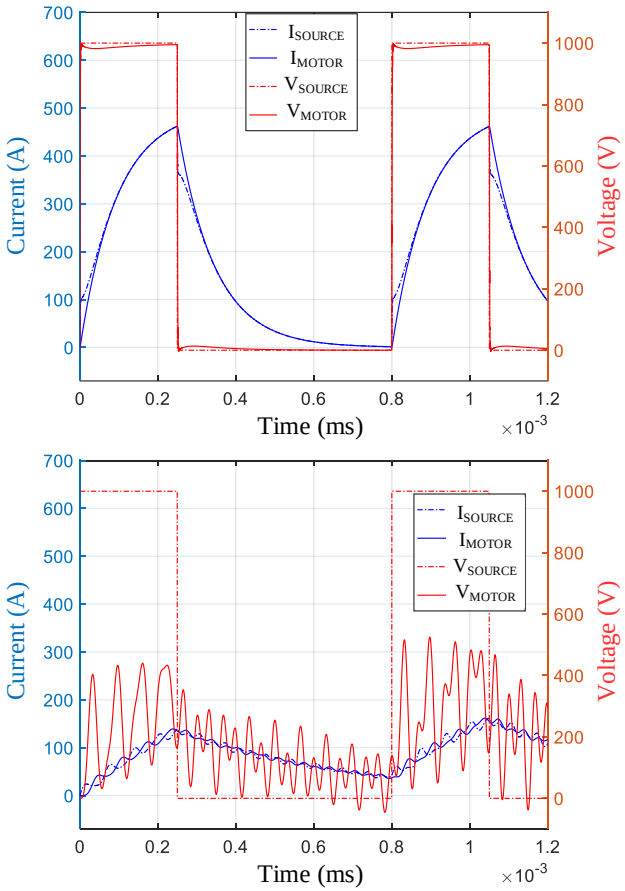

Fig. 6. Current (blue) and voltage (red) waveforms for pulses issued into the SRM system. Dashed lines are measured at the source, before the interconnecting cable. Solid lines are measured at the motor, after the interconnecting cable. Results are shown for a short interconnecting cable length of 1m (top) and a long interconnecting cable length of 2000 m (bottom).

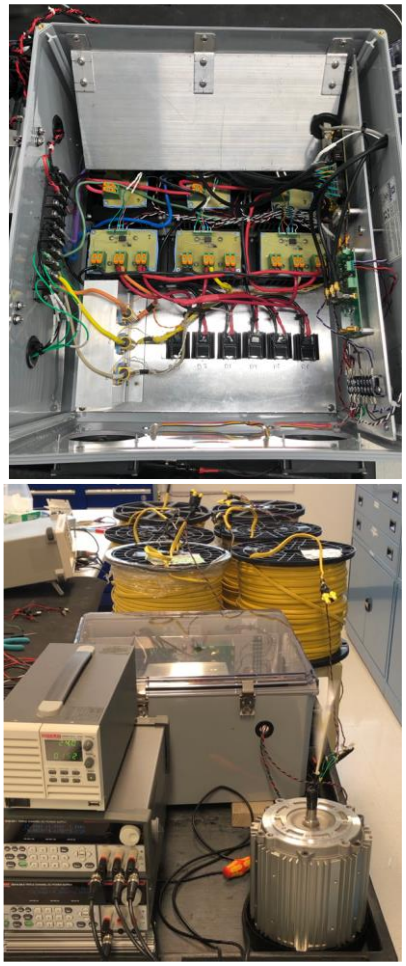

Fig. 7. (Top) Laboratory power converter test system utilizing the asymmetric half-bridge topology. (Bottom) Laboratory test system with switched reluctance motor at bottom right, power converter electronics at middle, and 1800 m of cable at top.

Thus, it is feasible to monitor the position of the rotor by monitoring the current in the excited coil.

The cabling between the power converter and the downhole motor has a strong effect on the voltage pulse waveform shape. This becomes more prominent with longer cable lengths, e.g., between a surface power converter and a downhole motor. The distributed inductances, capacitances, and resistances along the interconnect cabling act as reflecting elements for power transmitted through the cable.

The current waveforms, however, are largely unaffected as the power perturbations are largely from the resistive dissipation of voltages along the cable. This implies that, although voltage pulse waveforms issued into long interconnect cables can be highly nonlinear and superimposed with reflected voltage content from the distributed impedances along the cable, the current waveforms will maintain a stable relationship between the current issued by the power converter and the current through the motor coil. Any static differences in currents between the surface control system and the downhole motor system due to the interconnect cabling can be calibrated out of the system response. With this system simplification, it is feasible to control a SRM downhole over long cable lengths by monitoring the current supplied by a surface power converter system.

III. SWITCHED RELUCTANCE MOTOR SIMULATION

A system model was developed to evaluate the voltage and currents of the power source and the motor system. The interconnect cabling was modeled as a continuum of distributed impedances, Fig. 5. The voltages and currents as a function of time for every node in the system were calculated using a finite difference model based on a state space representation of the system. In this model, the state space representation of the currents and voltages in the distributed cable impedance are:

$$\dot{x} = Ax + BU \tag{2}$$

where $x = [i_1 \quad \cdots \quad i_N]$ is the state vector of currents flowing through each discrete circuit element $1, \ldots, N$ in the distributed cable model, $\dot{x} = \left[\frac{di_1}{dt} \quad \cdots \quad \frac{di_N}{dt}\right]$ is the first derivative w.r.t. time of the currents in the state vector, A is the $N \times N$ state transition matrix containing coefficients associated with the currents through each discrete element derived from the voltage loop at each distributed element in the model, $U = \frac{dV_S}{dt}$ is the source vector containing the derivative w.r.t. time of the surface excitation voltage source, and B is the $1 \times N$ source transition matrix containing coefficients associated with the voltage derivative derived from the voltage loop at each distributed element in the

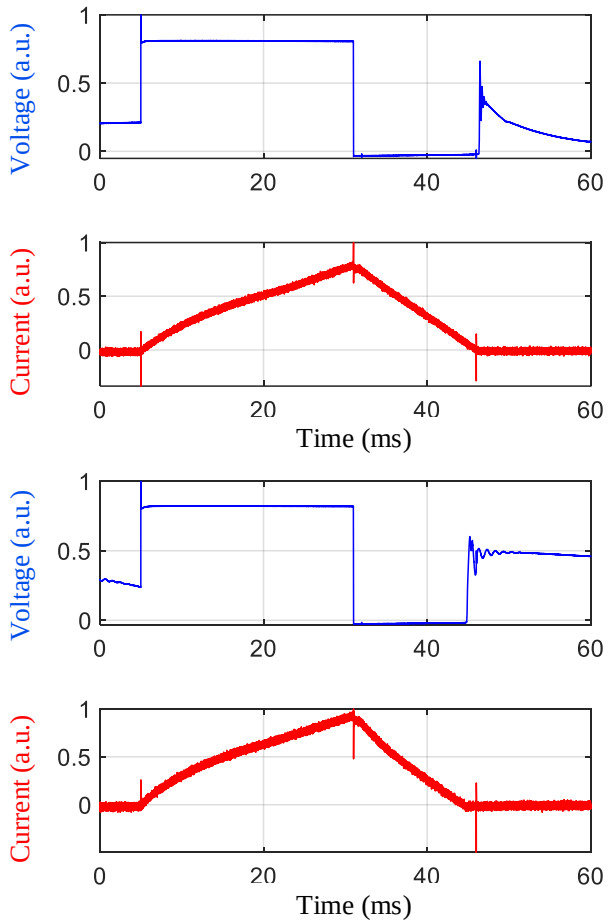

Fig. 8. Voltage, blue, and current, red, waveforms measured at the power source during the switched reluctance motor laboratory demonstration while the motor was operating. The short cable configuration (top) and the long cable configuration (bottom) show difference in the ringdown behavior of the voltage waveforms, but substantially the same current waveforms.

model. For a time step Δt, the forward difference estimate of $x(t+\Delta t)$ from a prior time $x(t)$ is:

$$x(t+\Delta t) = x(t) + \dot{x}(t)\cdot\Delta t \quad (3)$$

Similarly, the estimate of $U(t)$ from a known $V_S(t+\Delta t)$ and a prior time $V_S(t)$ is:

$$U(t)\cdot\Delta t = V_S(t+\Delta t) - V_S(t) \quad (4)$$

Combining equations (2)-(4), the currents through each discrete element as time is advanced by Δt is then:

$$x(t+\Delta t) = (I + A\cdot\Delta t)\cdot x(t) + B\cdot U(t)\cdot\Delta t \quad (5)$$

where I is an $N\times N$ identity matrix. The state space model successively solves for all currents through each discrete element, advances time by some small increment Δt, then updates the solution with the currents through each discrete element at this new time step.

Voltage pulses with a magnitude of 1kV, an "on-time" of 250µs, and a repetition rate of 625 Hz were injected into the cable/motor system. The motor coils were modeled with series resistance $R_M = 0.8\ \Omega$ and a rotor-position dependent inductance profile that ranged from a minimum of $L_M = 1.85\ mH$ to a maximum of $L_M = 9.25\ mH$. The distributed element parameters for the cable were values typical for an ESP umbilical: parallel capacitance $C_P = 78\,\mu F/m$, series inductance $L_S = 1.2\ \mu H/m$, series resistance $R_S = 5.5\ m\Omega/m$, and parallel conductance of $G_P = 0.1\ mS/m$.

Short and long cable results are shown in Figure 6. The short cable model was 1 m in length. The long cable model was 2000 m in length. In the short cable model, Fig. 6 top, the high voltage source is exciting the coil from 0 to 250 µs, and the current in the coil is in the building state. At 250 µs, both the inlet and return lines into the coil are grounded, and the current is in the sustaining state. At 800 µs, the process repeats and the high voltage source once again excites the coil. In this short cable model, the voltages and currents at the motor and the source are nearly identical. Only minor differences can be seen, mostly due to dissipative losses from the resistance and inductance of the coil itself. The current waveform at the surface can be easily used to monitor the current waveform at the motor, and hence used as a means of closed loop control.

In the long cable model, Fig. 6 bottom, the same voltage pulse excitation is used. In this model, there is clearly a difference in the voltage waveforms at the source and at the motor. The ringing behavior is due in large part to reflections from the distributed impedances of the cable. The current waveforms at the motor and the source are nearly identical. Some minor oscillation occurs due to dynamic impedance effects of the cable as the voltage waveforms swing, but the overall trend remains the same. Note that the current sourced by the source is reduced in the long cable case, as the 2000 m length of cable adds series resistance to the system and thus reduces the amount of current able to be supplied. This model shows the current waveforms at the surface can be used to monitor the current waveforms at the motor, even in the case of a long cable, and hence used as a means of closed loop control. Submersion of the cabling will have little to no effect on the performance of the system, as it will only modify the conductivity of the material surrounding the cable exterior, e.g. G_P will decrease slightly as the outer jacket material of the cable bundle will be surrounded by mixtures of brine an oil rather than air but will still be much larger than the effective impedance of C_P at operating frequencies.

IV. SWITCHED RELUCTANCE MOTOR LAB TESTING

This current measurement concept was evaluated in a laboratory test, with a short cable length of 1 m and a long cable length of 1800 m, with the lab setup shown in Fig. 7. The laboratory system was configured in the same manner as Figure 3. The SRM was a 12/8 SRM design with coil resistance of 8.1Ω and inductance ranging from a minimum of 90 mH to a maximum of 310 mH. The 1800 m length of cable had a lumped series resistance of 5Ω, a lumped series inductance of 183 mH, and a lumped parallel capacitance of 76 nF. Pulsing sequences were issued into the motor to rotate it at a constant rate. The power converter voltages and currents measured during rotation are shown in Fig. 8.

In the short cable case, Fig. 8 top, the power converter issues voltage pulses from 5-30 ms and the coil current is in the building state. The state then changes, and the current in the coil decays. The voltage and current waveforms behave as expected for this cabling configuration. The subsequent rise in voltage is due to pulsing action in a neighboring coil,

though the current stays at zero as this coil is no longer being excited. In the long cable case, Fig. 8 bottom, the power converter state timing is the same as the short cable case. The voltage waveforms show reflections during the transition at 55 ms. This is more prominent in the long cable case, as the distributed impedances of the long cable become more significant for the way the motor is driven. The current waveforms remain predictable, and immune from any large swings that the voltage waveforms experience. This matches well with the system model results shown above.

V. OUTLOOK AND CONCLUSIONS

Switched reluctance motors have advantages over conventional PMM and IM systems as the as the primary motor in an electric submersible pump. In this unique downhole application, long cabling in excess of 1km is required between surface power converter systems and the downhole motor. SRM systems require well timed pulse waveforms to properly rotate, oftentimes requiring downhole sensors to monitor motor characteristics. It was demonstrated that current waveforms on the motor coil excitation conductors at the surface can be utilized as a source of motor performance feedback and control which are insensitive to the highly unpredictable behavior of the voltage waveforms.

A state-space model of the surface controller, interconnect cabling, and motor system showed the behavior of the unpredictable voltage waveforms, as well as the stable behavior of the surface current waveforms. The stable behavior of these current waveforms, even in the case of 2km long interconnect cabling, can be used a reliable source of feedback for the downhole motor characteristics. A laboratory demonstration of the system showed excellent agreement with the voltage and current waveforms predicted by the state-space model, and further validated the use of surface current waveforms for motor control. SRMs are a promising technology that may increase the reliability of ESP systems used in oil & gas applications worldwide.

REFERENCES

[1] W.A. Limanowka, S. Degen, and G. Benwell, “Preventive Maintenance of Electric Submersible Pumps and its Relationship to Root Cause of Failure Analysis.” *Can. Int. Petr. Conf.,* Alberta, CA, June 2000. PETSOC-2000-035.

[2] E.R. Upchurch, “Analyzing Electric Submersible Pump Failures in the East Wilmington Field of California.” *SPE ATCE*, New Orleans, USA, September 1990. SPE-20675-MS.

[3] M.O. Durham, J.H. Williams, D.J. Goldman, “Effect of Vibration on Electric-Submersible Pump Failures.” *J. Pet. Technol*. (02) pp. 186-190. SPE-16924-PA.

[4] E. Bostanci, et. al., “Opportunities and Challenges of Switched Reluctance Motor Drives for Electric Propulsion: A Comparative Study.” *IEEE Trans. Transp. Elect.* (3) 1, pp. 58-75, March 2001.

[5] M.R. Harris, and T.J.E. Miller, "Comparison of design and performance parameters in switched reluctance and induction motors." *Fourth Int. Conf. Elect. Mach. and Drives Conf.*, pp. 303-307, IET, 1989.

[6] N. Yan, X. Cao, and Z. Deng. "Direct torque control for switched reluctance motor to obtain high torque–ampere ratio." *IEEE Transactions on Industrial Electronics* 66.7 (2018): 5144-5152.

[7] J. Zhu, K.W.E. Cheng, and X. Xue. "Design and analysis of a new enhanced torque hybrid switched reluctance motor." *IEEE Transactions on Energy Conversion* 33.4 (2018): 1965-1977.

[8] A.V. Radun, “Design Considerations for the Switched Reluctance Motor.” *IEEE Trans. Ind. Appl.* (31) 5, pp. 1079-1087, September,1995

[9] A.V. Radun, “Analytically Computing the Flux Linked by a Switched Reluctance Motor Phase When the Stator and Rotor Poles Overlap.” *IEEE Trans. Magn.* (36) 4, pp. 1996-2003, July 2000.

[10] P.J. Lawrenson, et. al., “Variable-Speed Switched Reluctance Motors.” *IEEE PROC* (127) 4, pp. 253-265, July 1980.

[11] M. Ilic’-Spong, et. al., “Feedback Linearizing Control of Switched Reluctance Motors.” *IEEE Trans. Auto. Cntrl.* (AC-32) 5, pp. 371-379, May 1987.

[12] P.C. Kjaer, J.J. Gribble, and T.J.E. Miller, “High-Grade Control of Switched Reluctance Machines.” *IEEE IAS* (1) pp. 92-100, 1996.

[13] J.H. Kim, and R.Y. Kim. "Sensorless direct torque control using the inductance inflection point for a switched reluctance motor." *IEEE Transactions on Industrial Electronics* 65.12 (2018): 9336-9345.

[14] T.R. Brinner, R.H. McCoy, and T. Kopecky. "Induction versus permanent-magnet motors for electric submersible pump field and laboratory comparisons." *IEEE Transactions on Industry Applications* 50.1 (2013): 174-181.

[15] K. Vijayakumar, et. al., "Switched Reluctance Motor Modeling, Design, Simulation, and Analysis: A Comprehensive Review." *IEEE Trans. Mag.* (44) 12, pp. 4605-4617, December 2008.

[16] S.M. Mahmoud, et. al., “Studying Different Types of Power Converters Fed Switched Reluctance Motor.” *Int. J. Elect. & Elec. Eng.* (1) 4, pp. 281-290, December 2013.